ACS APPLIED MATERIALS & INTERFACES

Surfaces, Interfaces, and Applications

Electrochemical Analysis of Target-Induced Hairpin-Mediated Aptamer Sensors

Shao Su, Jianfeng Ma, Yongqiang Xu, Hemeng Pan, Dan Zhu, Jie Chao, Lixing Weng, and Lianhui Wang

ACS Appl. Mater. Interfaces, **Just Accepted Manuscript** • DOI: 10.1021/acsami.0c12897 • Publication Date (Web): 21 Sep 2020

is published by the American Chemical Society. 1155 Sixteenth Street N.W., Washington, DC 20036

Electrochemical Analysis of Target-Induced Hairpin-Mediated Aptamer Sensors

Shao Su[1], Jianfeng Ma[1], Yongqiang Xu[1], Hemeng Pan[1], Dan Zhu[1], Jie Chao[1], Lixing Weng[1, 2, *], Lianhui Wang[1, *]

[1]Key Laboratory for Organic Electronics and Information Displays (KLOEID) & Jiangsu Key Laboratory for Biosensors, Institute of Advanced Materials (IAM), National Synergetic Innovation Center for Advanced Materials (SICAM), Nanjing University of Posts and Telecommunications, 9 Wenyuan Road, Nanjing 210023, China.

[2]College of Geography and Biological Information, Nanjing University of Posts & Telecommunications, Nanjing 210023, China.

ABSTRACT: The state of probe DNA on the biosensing interface greatly affect the detection performance of electrochemical DNA biosensors. Herein, we constructed a target-induced hairpin-mediated biosensing interface to study the effect of probe DNA on the analytical performance of adenosine triphosphate aptamer (ATPA) and adenosine triphosphate (ATP) detection. Moreover, we also explored the electrochemical contribution of co-existed hairpin and double-strand DNA (dsDNA) on this sensing interface. Experimental results suggested that the molecular recognition ability and detection performance of biosensing interface were majorly dependent on the surface density of methylene blue (MB)-labelled probe hairpin DNA and partly affect by the spatial state of the formed dsDNA. When the surface density of hairpin DNA was moderate (5.72 pmol·cm^{-2}), this sensing interface determine as low as 0.74 fM ATPA and 5.04 pM ATP with high selectivity and excellent regeneration, respectively. Furthermore, we calculated that the formed dsDNA had 31.87% contribution in total electrochemical signal for 10 pM ATPA detection. Based on above results, we designed a XOR logic gate based on the biosensing interface for ATPA and ATP detection.

KEYWORDS: biosensing interface, electrochemical biosensor, aptamer, adenosine triphosphate, logic gate.

INTRODUCTION

Electrochemical DNA biosensors[1-5] have many advantages included excellent sensitivity, high selectivity, low cost, and good portability, stability, and reproducibility[5-13], which are promising tools for quantitative detection of disease-related biomolecules[14-16], environmental pollutants[17,18], pathogenic microorganisms[19, 20] and tumor cells[21-24]. As we know, the detection performance of electrochemical DNA biosensors greatly depends on the length[19, 25], composition[26], surface density[27-29] and spatial state[30-32] of probe DNA. Generally, high surface density often brings excellent molecular recognition ability on a biointerface. However, it often limits the analytical performance due to the poor hybridization efficiency[19, 28]. An exciting finding is the favorable spatial arrangement of probe DNA with suitable surface density can brings a satisfactory analytical performance on a biosensing interface[33, 34]. Therefore, many groups have devoted to exploring better analytical performance by regulating interface state of probe DNA. For example, Gu et al. reported that the interfacial interaction and molecular recognition were dependent on the spatial organization of probe DNA, which was regulated by the probe surface density[32]. Lin et al. also reported that the hybridization efficiency was interrelated with the surface density of probe DNA by tuning the size of tetrahedral DNA nanostructures (TDNs) [34]. Though many advances of biosensing interfaces were achieved, it is still a challenge to construct an ideal biosensing interface with high analytical performance.

Since the stem-loop DNA structure (also called hairpin structure) was introduced into the construction of an electrochemical DNA sensor by Fan et al., it has attracted great increasing research interests in electrochemical sensors[35]. A popular method is labelled a redox reporter on the hairpin structure to monitor the molecular recognition process and analytical performance. Many groups also used redox reporter-labelled hairpin structures to investigate the influences factors of electrochemical responses[35-37]. For instance, Plaxco and co-workers systematically studied the effect of probe density and target length of molecular beacon on signal responses of the electrochemical DNA sensor[38]. They pointed out that the redox reporter closed to electrode surface and generated electrochemical signal. Recently, the same group reported that the electron transfer was dependent on the distance between the electrochemical indicator bound double-stranded DNA (dsDNA) and electrode surface, which obeyed a contact-mediated mechanism[31]. As we know, this distance is also influenced by neighboring probe DNA and captures biomarkers. For hairpin-

mediated biointerface, the opened hairpin DNA and the formed double-strand DNA (dsDNA) were adjusted by the addition of target DNA concentration, making them coexist on the biointerface. Therefore, redox reporter labelled on both hairpin DNA and the formed dsDNA generate electrochemical signals. An interesting question is emerging, what about the electrochemical contribution of coexisted hairpin DNA and dsDNA and analytical performance of this biosensing interface?

In response, we designed a target-induced hairpin-mediated biointerface to characterize its analytical performance and study the electrochemical contribution of different interface components. As shown in Scheme 1, hairpin DNA labelled with methylene blue (MB) was assembled on gold electrode surface. At first, only hairpin DNA was assembled on gold electrode surface, suggesting that the electrochemical reaction was a typical surface-controlled process (Fig. S1). Then, the designed hairpin DNA was opened and dsDNA was formed after adding adenosine triphosphate aptamer (ATPA). The amount of dsDNA increased with the increasing ATPA concentration. Finally, all hairpin DNA structures switched to dsDNA. At this moment, it gradually turned to diffusion-limited reaction. When hairpin DNA and dsDNA simultaneously existed on electrode surface, the formed dsDNA was easily influenced by the neighboring hairpin probe and generated a tilting angle between upright dsDNA and electrode surface because of the steric effect of hairpin DNA and the flexibility of dsDNA. As a result, the distance between electrochemical indicator (MB) and the electrode surface changed with the content of hairpin and dsDNA, which can affect electrochemical signal. In other words, the MB-labelled dsDNA also contributed electrochemical responses, which greatly depended on the state of the remaining hairpin DNA and the formed dsDNA on the biosensing interface. In contrast, dsDNA could switch back to hairpin structure with the addition of ATP because aptamer can specifically recognize ATP. Therefore, we can efficiently analyze ATPA and ATP according to the configuration change. We also can regulate the ratio of dsDNA and hairpin DNA on the sensing interface to study their electrochemical contribution.

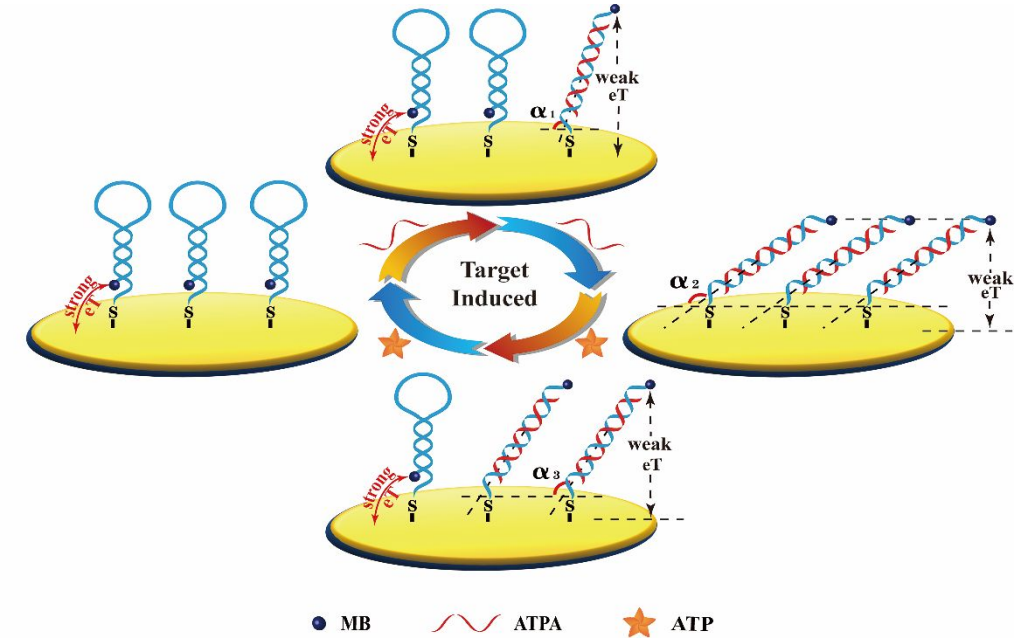

Scheme 1. Schematic of target-induced hairpin-mediated sensing interface for ATP aptamer (ATPA) and ATP analysis. The hairpin DNA was opened to dsDNA with the addition of ATPA. A titling angle (α) was obtained from dsDNA and electrode surface due to the steric effect of hairpin DNA and the flexibility of dsDNA. After adding ATP, ATPA preferentially reacted with ATP and released from dsDNA. The left probe DNA switched back to hairpin DNA with the help of Mg^{2+}.

EXPERIMENTAL SECTION

Reagents. All the information of reagents were listed in supporting information.

Preparation of Hairpin-Mediated Sensing Interface. A classical cleaning method was used to treat gold electrode[39]. After cleaning, hairpin/Au electrode was obtained by incubating MB-labelled hairpin DNA solution onto the cleaned gold electrode at 37ºC overnight. After washing the unbound hairpin DNA, 6-mercaptohexanol (MCH) blocked the remaining active spots of hairpin/Au electrode at 37ºC for 1 h. Finally, ATPA or ATP detection performance and electrochemical contribution of dsDNA were studied at the MCH/hairpin/Au.

Dynamic Study of Probe Surface Density. Different concentrations (5 μM, 1 μM and 0.1 μM) of MB-labelled hairpin DNA were immobilized on electrode surface to obtain high, moderate and low probe surface density. The dynamic study of surface density was studied by reacting different ATPA concentrations (1 fM-100 nM) at hairpin/Au sensing interface. The addition of ATPA simultaneously decreased the hairpin DNA surface density and increased the amounts of dsDNA.

RESULTS AND DISCUSSIONS

The Feasibility of Target-Induced Hairpin-Mediated Biosensing Interface

The feasibility of target-induced hairpin-mediated biosensing interface was tested by differential pulse voltammetry (DPV), cyclic voltammetry (CV) and electrochemical impedance spectroscopy (EIS). Fig. S2 showed the CV curves of different electrodes in $[Fe(CN)_6]^{3-/4-}$ solution. Obviously, the peak currents of hairpin/Au (curve b) were smaller and the peak separation became larger than those of bare Au (curve a), indicating that the successful immobilization of hairpin on electrode surface. The peak currents of ATPA/hairpin/Au increased with the addition of ATPA (curve c), suggesting that electron transfer was facilitated during the conversion from hairpin DNA to dsDNA. In contrast, the addition of ATP made the peak currents of ATPA/hairpin/Au decrease (curve d), which was ascribed to the formation of hairpin structure. The corresponding EIS were listed in Fig. 1A, which also supported this conclusion. The electron-transfer resistance of bare gold electrode (curve a, R_{ct}=222.6 Ω) was much smaller than that of hairpin/Au electrode (curve b, R_{ct}=16995.7 Ω), which was ascribed to the immobilization of hairpin DNA. With the addition of ATPA, the R_{ct} decreased with the formation of dsDNA (curve c, R_{ct}=11896.1 Ω). In contrast, the addition of ATP leaded to the increment of the R_{ct} (curve d, R_{ct}=14260.2 Ω). Obviously, the value of R_{ct} was greatly dependent on the surface density of hairpin DNA and the formed dsDNA. The DPV (Fig. 1B) results of different electrodes also proved the successful construction of hairpin-mediated biosensing interface. The peak currents of MB decreased with the addition of ATPA (curve b) and recovered with ATP addition (curve c). We further used atomic force microscopy (AFM) to characterize the change from hairpin DNA to dsDNA with the addition of ATPA. The length increased from 11 ± 0.4 nm to 8 ± 0.2 nm with hairpin DNA switching to dsDNA, proving the successful construction of target-induced biosensing interface (Fig. S3). All data suggested that hairpin DNA and dsDNA assembled on sensing interface can be easily adjusted by the addition of ATPA and ATP.

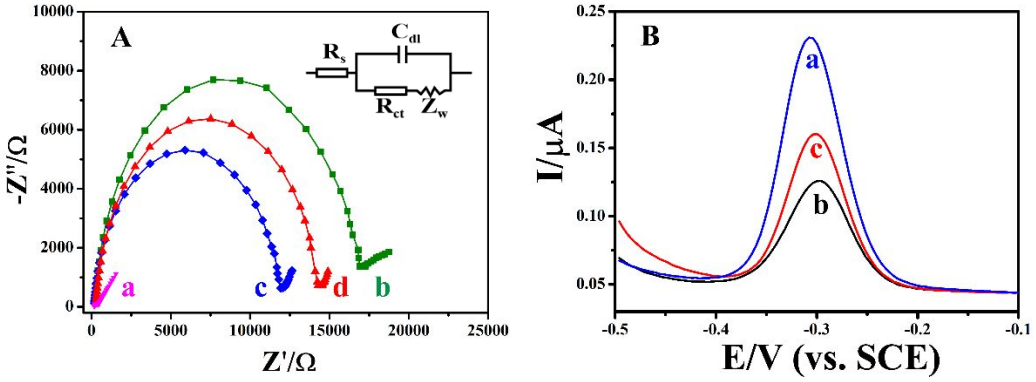

Figure 1. (A) The EIS characterization of (a) bare Au electrode, (b) hairpin/Au, (c) ATPA/hairpin/Au and (d) ATP/ATPA/hairpin/Au. Inset: an analog circuit of the EIS. (B) The DPV signals of (a) hairpin/Au, (b) ATPA/hairpin/Au and (c) ATP/ATPA/hairpin/Au.

Analytical Performance of the Sensing Interface

On the concept of sensing application, we tested the analytical performance of hairpin-mediated sensing interface for the detection of ATPA and ATP. Fig. 2A showed that the DPV signals suppressed with the increasing ATPA concentration ranging from 1 fM to 100 nM. Obviously, the DPV responses reached a plateau when ATPA concentration was 100 nM. As a result, the signal suppression rate ($\Delta I/I_{initial}$, $\Delta I=I_{APTA}-I_{initial}$) was linear with the logarithm of 1 fM-10 nM ATPA (Figure 2B). The corresponding equation was obtained as $y=6.964x + 10.590$ ($R^2=0.997$) and the detection limit was estimated as 0.74 fM. In contrast, the formed dsDNA can switch back to hairpin DNA structure after the addition of ATP with Mg^{2+}-assisted. The added ATP preferentially reacted with ATPA due to the specific binding reaction and the left probe DNA formed hairpin structure again[40]. Therefore, the DPV signals increased with the addition of 10 pM-5 nM ATP (Figure 2C). Similarly, the signal recovery rate ($\Delta I/I_{ATPA}$, $\Delta I=I_{ATP}-I_{ATPA}$) was linear with the logarithm of 10 pM-5 nM ATP with a detection limit of 5.04 pM (Figure 2D). Besides excellent sensitivity, this sensing interface also displayed extraordinary selectivity, which can efficiently distinguish single-based mismatch DNA sequence (Fig. S4A) and CTP, GTP (Fig. S4B), respectively. Moreover, the electrochemical signal only decreased 0.27% for ATPA detection after 5 times repeated use, indicating that this biosensing interface also displayed excellent regeneration (Fig. S5).

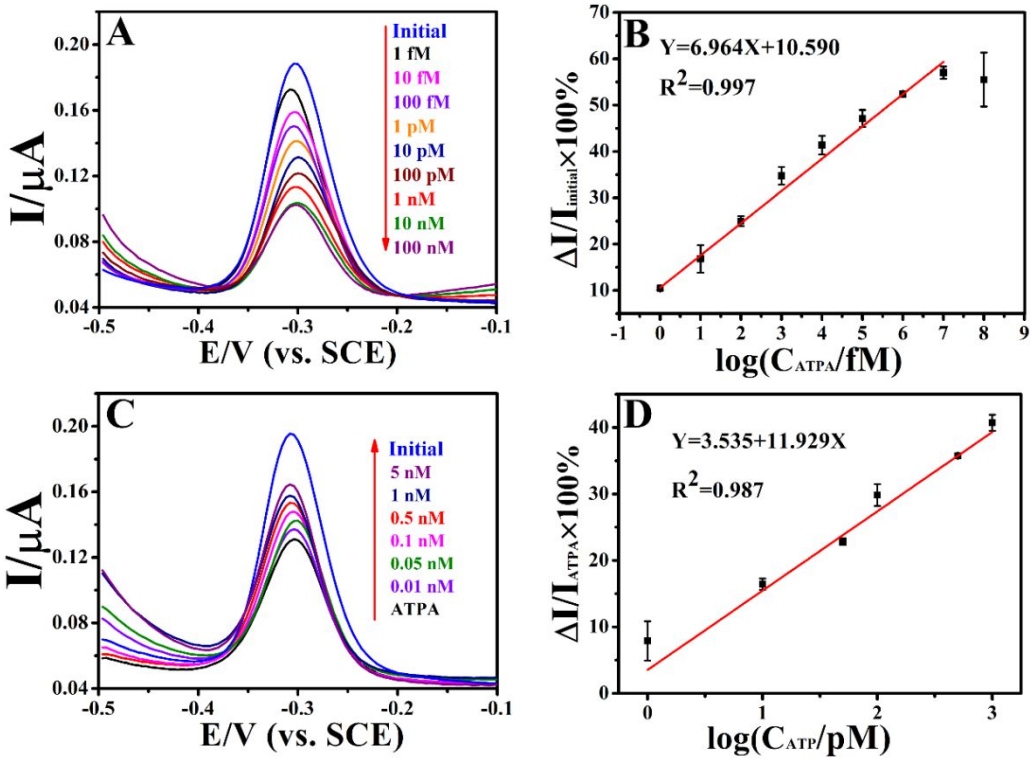

Figure 2. The results for ATPA and ATP detection by using the designed sensing interface, respectively. (A) The DPV signals of this sensing interface for different ATPA concentrations detection. (B) The signal suppression rate ($\Delta I/I_{inital}$) changed with the increasing ATPA concentration. (C) DPV curves of sensing interface for different ATP concentration detection ranging from 0.01 nM-5 nM. (D) The corresponding signal recovery rate (($\Delta I/I_{ATPA}$)) changed with ATP concentration.

Detection Dynamic Range of Probe Surface Density for APTA Detection

Surface density of probe DNA greatly affect the analytical performance of electrochemical biosensors[41]. Taking ATPA detection as an example, we selected three concentrations (0.1 μM, 1 μM and 5 μM) of hairpin DNA assembled on gold electrode surface to study the effect of surface density on the analytical performance. Obviously, the peak current and surface coverage of this sensing interface changed with the concentrations of probe DNA (Fig. S6). As exhibited in Fig. 3A, the low concentration of probe DNA (0.1 μM, 1.43 pmol·cm^{-2}) led to a narrow linear range (1 fM-1 pM) and low peak currents. As we know, low concentration of probe DNA assembled on gold electrode surface has enough space for capturing target ATPA and litter steric hindrance from neighboring hairpin DNA. However, the flexibility of dsDNA made the formed dsDNA tilte on the gold electrode surface, which may hinder target ATPA to react with the remaining hairpin DNA. At high hairpin DNA concentration (5 μM, 8.71

pmol·cm^{-2}, Fig. 3C), higher electrochemical responses were observed. However, the analysis performance (100 fM-10 nM) was worse than that obtained with moderate probe surface density. Expectedly, the moderate surface density (1 μM, 5.72 pmol·cm^{-2}) of hairpin DNA exhibited wider linear range (1 fM-10 nM, Fig. 3B). As we know, if the density of probe DNA is too dense, the hybridization reaction will become difficult due to the electrostatic repulsive force between the negatively charge probe DNA and target DNA. In addition, the steric hindrance also affects the hybridization reaction because it occurs at the solid-liquid interface. Therefore, a suitable surface density of probe DNA can bring the better detection performance.

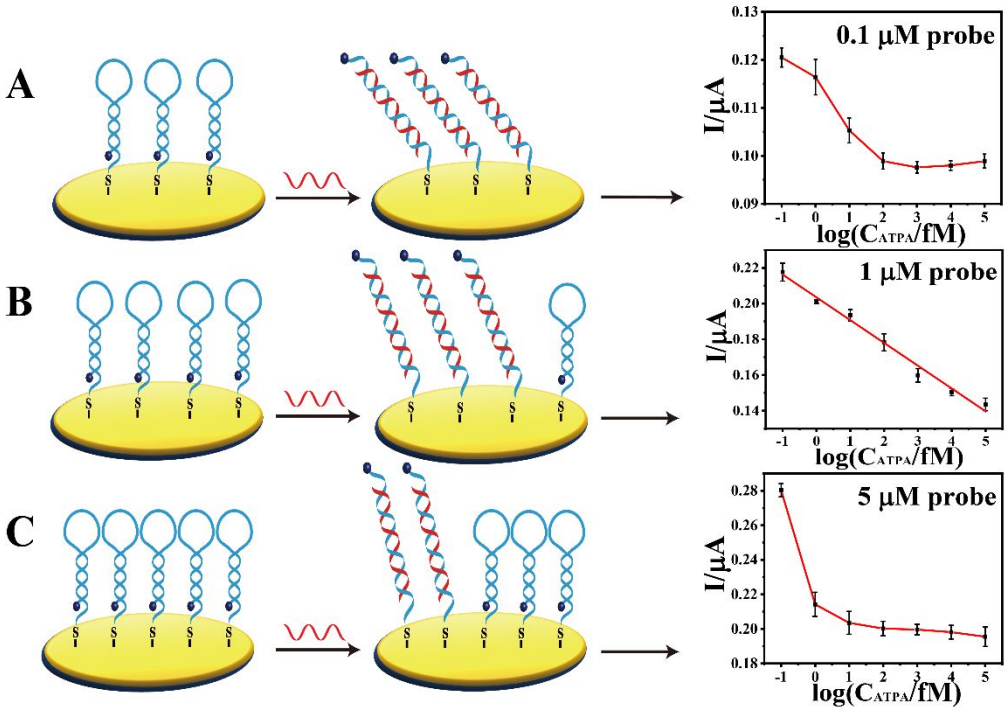

Figure 3. The dynamic study of hairpin DNA probe for ATPA detection with different DNA surface density. (A) Low probe surface density (0.1 μM) for APTA detection. (B) Moderate probe surface density (1 μM) for APTA detection. (C) High probe surface density (5 μM) for APTA detection.

Electrochemical Contribution of Coexisted Hairpin DNA and dsDNA on Sensing Interface

The designed sensing interface showed excellent analytical performance for ATPA and ATP detection. One problem is that the contribution of the formed double-stranded DNA in electrochemical signals during the ATPA detection. Therefore, we tested the effect of coexisted hairpin DNA and dsDNA on the electrochemical responses. As published, hairpin DNA assembled on sensing interface for target molecules detection has three stages: (1) only hairpin DNA, (2) coexisted hairpin DNA and dsDNA, and (3) almost only dsDNA[42, 43]. Up to now, most groups focus

on studying the effect of stage 1 or stage 3 on the electrochemical responses. The intermediate state of coexisted hairpin DNA and dsDNA was still not clear. Especially, the contribution of hairpin DNA or dsDNA to electrochemical signal should be understood. It is well-known that the electrochemical response of redox reporter-labelled hairpin DNA or dsDNA on sensing interface was dependent on the distance between the electrochemical indicator and electrode surface, which obeyed a contact-mediated mechanism[31]. As a result, the coexisted hairpin DNA and dsDNA have simultaneously contributed to the electrochemical signals, which greatly affect the analytical performance for ATPA detection.

As illustrated in Scheme 1, the amount of hairpin DNA decreased and the number of dsDNA increased with the addition of ATPA, resulting in the electrochemical signal of MB decreasing (Fig. 4A). Obviously, the ratio of hairpin DNA and dsDNA on sensing interface was easily regulated by the addition of APTA concentration. Moreover, a tilting angle was obtained due to the flexibility of dsDNA and the steric effect of hairpin DNA. At this moment, the peak current of sensing interface was contributed by the remaining hairpin DNA ($I'_{hairpin}$) and the formed dsDNA (I_{dsDNA}). Therefore, the equation of electrochemical response was listed as following:

$$I_{DNA} = I'_{hairpin} + I_{dsDNA} \qquad (1)$$

It should be noted that the peak current of initial sensing interface ($I_{hairpin}$) was fixed when probe hairpin DNA was assembled on electrode surface. Therefore, we employed $I_{hairpin}$ as a standard to evaluate the peak current of intermediate state (I_{DNA}). According to the previous works[42, 44], the calculation process was listed in Supporting Information. Finally, $I_{DNA}/I_{hairpin}$ can be expressed as:

$$\frac{I_{DNA}}{I_{hairpin}} = \frac{\Gamma_1}{\Gamma} + \frac{0.2\Gamma_2 D_{MB}^{\frac{1}{2}}}{\Gamma \cos\alpha} v^{-\frac{1}{2}} \qquad (2)$$

Where Γ_1, Γ_2 and Γ are the surface coverage of hairpin DNA, dsDNA and coexisted hairpin DNA and dsDNA, respectively. α is the tilting angle between the formed dsDNA and gold electrode surface. v is the scan rate. It should be pointed out that probe hairpin DNA didn't fell off electrode surface, so the surface coverage of sensing interface was almost no change ($\Gamma_{hairpin}=\Gamma_{coexist}=\Gamma_1+\Gamma_2$). Therefore, $\frac{\Gamma_1}{\Gamma}$ is the contribution of the remaining hairpin DNA ($I'_{hairpin}$) in total electrochemical response (I_{DNA}), and the $\frac{\Gamma_2}{\Gamma}$ is the contribution of the formed dsDNA (I_{dsDNA}) in I_{DNA}.

As exhibited in Fig. 4B, if the concentration of ATPA was 10 fM, the ratio of peak current ($I_{DNA}/I_{hairpin}$) was almost no change when the scan rate was 0.05 $V \cdot s^{-1}$-0.4 $V \cdot s^{-1}$. If the scan rate

below 0.05 V/s, an obvious change of $I_{DNA}/I_{hairpin}$ was observed, suggesting that the formed MB-labelled dsDNA also contributed to the electrochemical signal at very low scan rate[36]. According to the equation 2, the electrochemical response was dominated by the MB-labelled hairpin DNA ($\frac{\Gamma_1}{\Gamma}$ =93.81%) and only 6.19% electrochemical response was contributed by the formed dsDNA. With the ATPA concentration increasing, more dsDNA formed and less hairpin DNA left. At this state, a linear relationship between $I_{DNA}/I_{hairpin}$ and $v^{-1/2}$ was listed in Fig. 3B, suggesting the electrochemical reaction was diffusion-limited process. In another word, the electrochemical signal was contributed by both MB-labelled hairpin DNA and MB-labelled dsDNA. Based on equation 2, the contribution of MB-labelled dsDNA increased to 31.87% when the ATPA concentration was 10 pM. Interestingly, the contribution of dsDNA decreased to 23.87% if we added 10 pM ATP into this detection strategy (Fig. S7), suggesting dsDNA switched back to hairpin DNA again.

For further understanding the reaction process, we investigated the electron transfer kinetics of different stages at sensing interface. According to Laviron theory,[45] the electron-transfer rate constant (k_s) was 14.64 s^{-1} when hairpin DNA was assembled on electrode surface (Fig. S1A, B). When the ATPA concentration was 10 pM, a part of hairpin DNA was opened to form dsDNA. At this moment, hairpin DNA and dsDNA coexisted at sensing interface, making the k_s decrease to 3.43 s^{-1} (Fig. S1C, D). If ATP added into this detection strategy, dsDNA switched back to hairpin structure. As a result, the k_s increased to 10.90 s^{-1} (Fig. S1E, F). Notably, the k_s of this hairpin-mediated sensing interface were larger than that of constructed by only dsDNA (2.25 s^{-1}, Fig. S8). The reason may be ascribed to the conversion efficiency of hairpin DNA to dsDNA isn't 100%.

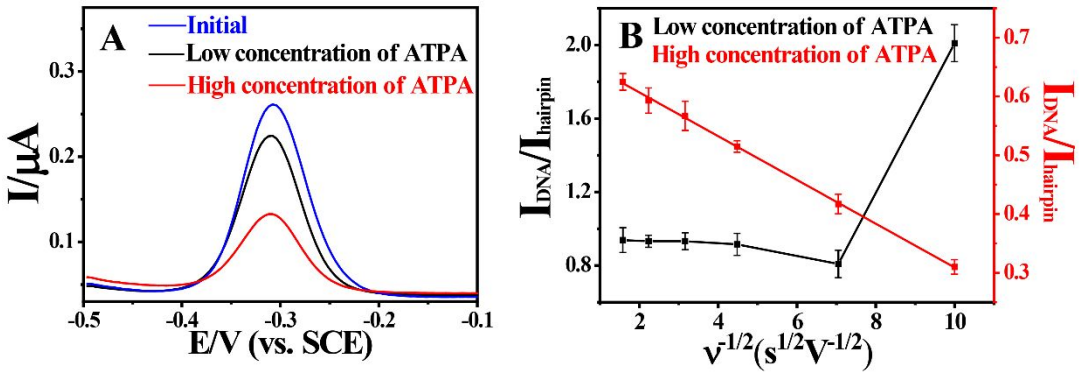

Figure 4. (A) DPV signals of hairpin DNA probe reacted with 10 fM (low concentration) and 10 pM (high concentration) ATPA, respectively, and (B) The relationship between peak current ratio ($I_{DNA}/I_{hairpin}$) and the inverse square root of scan rate ($v^{-1/2}$).

Construction of Logic Gate

Inspired by the remarkable detection performance of sensing interface with a moderate probe surface density, we designed a XOR logic gate based on the coexisted hairpin DNA and dsDNA sensing interface, where hairpin DNA for capturing ATPA and the formed dsDNA for binding ATP (Fig. 5A). Herein, we used ATPA and ATP as the inputs and the change of electrochemical signal (signal change%=$(I-I_{ATPA-1})/I_{ATPA-1}$) as output signals, respectively. The output signals with different inputs were shown in Fig. 5C. If added the same concentration of ATP and ATPA, the electrochemical signal was almost no change. As a result, the output was "0". The same output was also obtained when no target molecules added. If added ATP or ATPA, an obvious peak current change was observed (Fig. 5B). These results verified the XOR logic gate worked well.

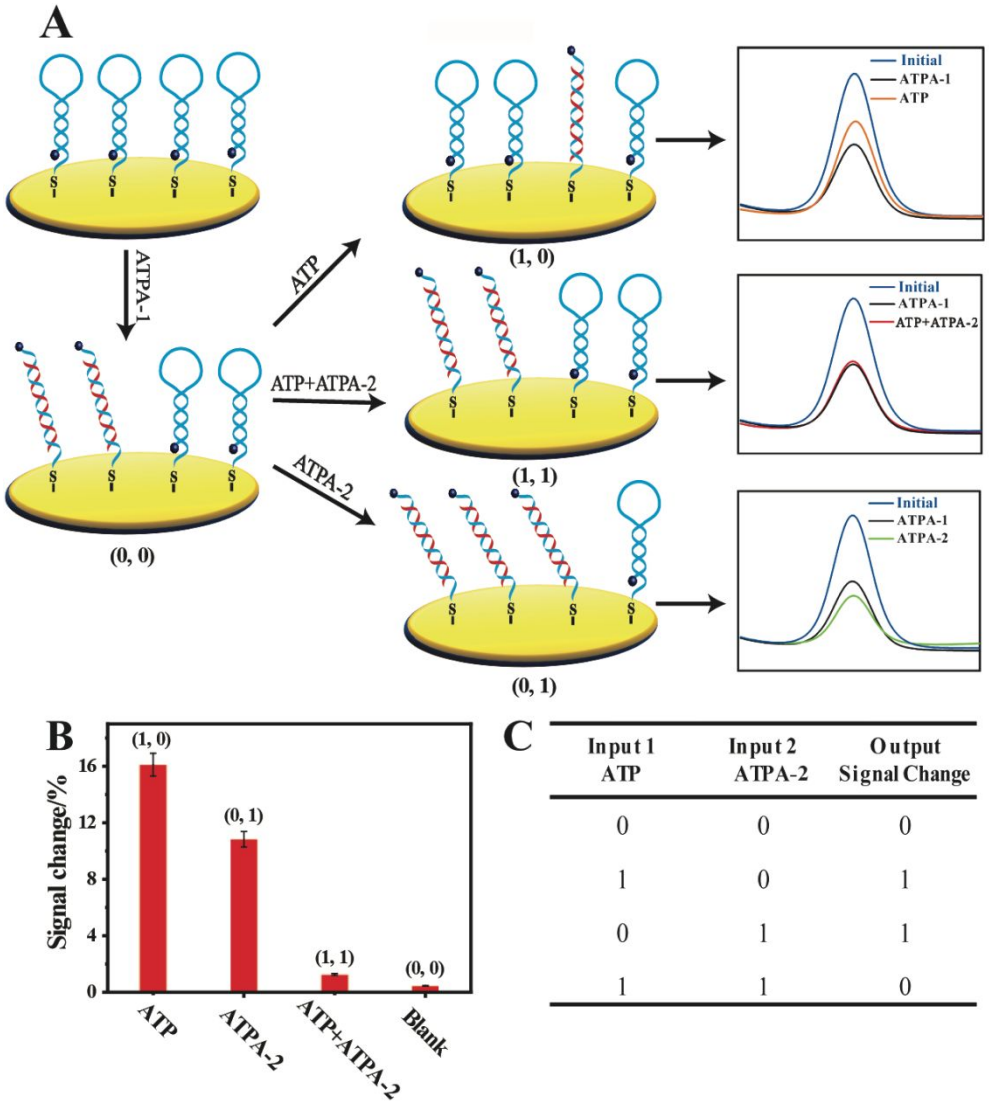

Input 1 ATP	Input 2 ATPA-2	Output Signal Change
0	0	0
1	0	1
0	1	1
1	1	0

Figure 5. XOR logic gate was designed based on target-induced hairpin-mediated sensing interface. (A) The schematic description of XOR logic gate construction and corresponding electrochemical

results. (B) The electrochemical signal change of XOR logic gate for ATPA and ATP detection. (C) The output signals were recorded with different inputs. If individually input ATPA or ATP, the input was defined as "1", otherwise was "0". The concentration of ATPA-1 and ATPA-2 were 1 nM and 100 nM, respectively. The ATP concentration was 500 pM.

CONCLUSION

In this work, we designed a target-induced hairpin-mediated sensing interface to explore the analytical performance and electrochemical contribution of hairpin DNA and dsDNA for the detection of aptamer sequence and ATP. Obviously, the moderate probe surface density (5.72 $pmol \cdot cm^{-2}$) led to better analytical performance. Moreover, the formed MB-labelled dsDNA also contributed to the electrochemical signal, which was dependent on the interface state included probe surface density and spatial arrangement. On the basis of above conclusion, a XOR logic gate was constructed when hairpin DNA and dsDNA coexisted on the sensing interface. All experimental data pave a way to understand the effect of interface state of redox-labeled DNA on analysis performance. It also provides a method for the design of sensors/biosensors.

Supporting Information

The Supporting Information is available free of charge via the Internet at http://pubs.acs.org.

The calculation process of electrochemical contribution and electron-transfer rate constant, CVs of different scan rate at sensing interface, CVs of different modified electrodes, AFM images of hairpin DNA and dsDNA, selectivity and reproducibility of designed sensing interface, surface coverage of different hairpin DNA concentration, peak current ratio ($I_{DNA}/I_{hairpin}$) at different stage of sensing interface and peak potential versus scan rate at sensing interface.

AUTHOR INFORMATION

Corresponding Author

Lixing Weng-College of Geography and Biological Information, Nanjing University of Posts & Telecommunications, Nanjing 210023, China.
Email: lxweng@njupt.edu.cn.
Lianhui Wang-Key Laboratory for Organic Electronics and Information Displays (KLOEID) & Jiangsu Key Laboratory for Biosensors, Institute of Advanced Materials (IAM), National Synergetic Innovation Center for Advanced Materials (SICAM), Nanjing University of Posts and Telecommunications, 9 Wenyuan Road, Nanjing 210023, China. orcid.org/0000-0001-9030-9172;
Email: iamlhwang@njupt.edu.cn.

Authors

Shao Su-Key Laboratory for Organic Electronics and Information Displays (KLOEID) & Jiangsu Key Laboratory for Biosensors, Institute of Advanced Materials (IAM), National Synergetic Innovation Center for Advanced Materials (SICAM), Nanjing University of Posts and Telecommunications, 9 Wenyuan Road, Nanjing 210023, China. orcid.org/0000-0002-9399-8249.

Jianfeng Ma-Key Laboratory for Organic Electronics and Information Displays (KLOEID) & Jiangsu Key Laboratory for Biosensors, Institute of Advanced Materials (IAM), National Synergetic Innovation Center for Advanced Materials (SICAM), Nanjing University of Posts and Telecommunications, 9 Wenyuan Road, Nanjing 210023, China.

Yongqiang Xu-Key Laboratory for Organic Electronics and Information Displays (KLOEID) & Jiangsu Key Laboratory for Biosensors, Institute of Advanced Materials (IAM), National Synergetic Innovation Center for Advanced Materials (SICAM), Nanjing University of Posts and Telecommunications, 9 Wenyuan Road, Nanjing 210023, China.

Hemeng Pan-Key Laboratory for Organic Electronics and Information Displays (KLOEID) & Jiangsu Key Laboratory for Biosensors, Institute of Advanced Materials (IAM), National Synergetic Innovation Center for Advanced Materials (SICAM), Nanjing University of Posts and Telecommunications, 9 Wenyuan Road, Nanjing 210023, China.

Dan Zhu-Key Laboratory for Organic Electronics and Information Displays (KLOEID) & Jiangsu Key Laboratory for Biosensors, Institute of Advanced Materials (IAM), National Synergetic Innovation Center for Advanced Materials (SICAM), Nanjing University of Posts and Telecommunications, 9 Wenyuan Road, Nanjing 210023, China.

Jie Chao-Key Laboratory for Organic Electronics and Information Displays (KLOEID) & Jiangsu Key Laboratory for Biosensors, Institute of Advanced Materials (IAM), National Synergetic Innovation Center for Advanced Materials (SICAM), Nanjing University of Posts and Telecommunications, 9 Wenyuan Road, Nanjing 210023, China. orcid.org/0000-0003-1030-9944.

Notes

The authors declare no competing financial interest.

ACKNOWLEDGEMENTS

This work was supported by the National Key Research and Development Program of China (2017YFA0205300), the National Natural Science Foundation of China (61671250 and 21475064),

the Program for Changjiang Scholars and Innovative Research Team in University (IRT_15R37), the Key Research and Development Program of Jiangsu (BE2018732), the Natural Science Key Fund for Colleges, Universities in Jiangsu Province (17KJA430011), the Priority Academic Program Development of Jiangsu Higher Education Institutions (PAPD, YX030003) and the Scientific Research Foundation of Nanjing University of Posts and Telecommunications (NY218032).

REFERENCES:

(1) Abi, A.; Lin, M.; Pei, H.; Fan, C.; Ferapontova, E. E.; Zuo, X. Electrochemical Switching with 3D DNA Tetrahedral Nanostructures Self-Assembled at Gold Electrodes. *ACS Appl. Mater. Interfaces* **2014**, *6* (11), 8928-8931.

(2) Chai, H.; Miao, P. Bipedal DNA Walker Based Electrochemical Genosensing Strategy. *Anal. Chem.* **2019**, *91* (8), 4953-4957.

(3) Kou, B.; Chai, Y.; Yuan, Y.; Yuan, R. Dynamical Regulation of Enzyme Cascade Amplification by a Regenerated DNA Nanotweezer for Ultrasensitive Electrochemical DNA Detection. *Anal. Chem.* **2018**, *90* (18), 10701-10706.

(4) Pei, H.; Lu, N.; Wen, Y.; Song, S.; Liu, Y.; Yan, H.; Fan, C. A DNA Nanostructure-Based Biomolecular Probe Carrier Platform for Electrochemical Biosensing. *Adv. Mater.* **2010**, *22* (42), 4754-4758.

(5) Lin, M.; Wen, Y.; Li, L.; Pei, H.; Liu, G.; Song, H.; Zuo, X.; Fan, C.; Huang, Q. Target-Responsive, DNA Nanostructure-Based E-DNA Sensor for MicroRNA Analysis. *Anal. Chem.* **2014**, *86* (5), 2285-2288.

(6) Feng, Q. M.; Zhao, X. L.; Guo, Y. H.; Liu, M. K.; Wang, P. Stochastic DNA Walker for Electrochemical Biosensing Sensitized with Gold Nanocages@Graphene Nanoribbons. *Biosens. Bioelectron.* **2018**, *108* (6), 97-102.

(7) Wen, Y. L.; Pei, H.; Shen, Y.; Xi, J. J.; Lin, M. H.; Lu, N.; Shen, X. Z.; Li, J.; Fan, C. H. DNA Nanostructure-Based Interfacial Engineering for PCR-Free Ultrasensitive Electrochemical Analysis of MicroRNA. *Sci. Rep.* **2012**, *2* (867), 2045-2322.

(8) Zhang, P.; Jiang, J.; Yuan, R.; Zhuo, Y.; Chai, Y. Highly Ordered and Field-Free 3D DNA Nanostructure: The Next Generation of DNA Nanomachine for Rapid Single-Step Sensing. *J. Am. Chem. Soc.* **2018**, *140* (30), 9361-9364.

(9) Zhang, X.; Yang, Z.; Chang, Y.; Qing, M.; Yuan, R.; Chai, Y. Novel 2D-DNA-Nanoprobe-Mediated Enzyme-Free-Target-Recycling Amplification for the Ultrasensitive Electrochemical Detection of MicroRNA. *Anal. Chem.* **2018**, *90* (15), 9538-9544.

(10) Zhou, F. Y.; Yao, Y.; Luo, J. J.; Zhang, X.; Zhang, Y.; Yin, D. Y.; Gao, F. L.; Wang, P. Proximity Hybridization-Regulated Catalytic DNA Hairpin Assembly for Electrochemical Immunoassay Based on in Situ DNA Template-Synthesized Pd Nanoparticles. *Anal. Chim. Acta* **2017**, *969* (5), 8-17.

(11) Xiong, E.; Zhang, X.; Liu, Y.; Zhou, J.; Yu, P.; Li, X.; Chen, J. Ultrasensitive Electrochemical Detection of Nucleic Acids Based on the Dual-Signaling Electrochemical Ratiometric Method and

Exonuclease III-Assisted Target Recycling Amplification Strategy. *Anal. Chem.* **2015**, *87* (14), 7291-7296.

(12) Yu, S.; Wang, Y.; Jiang, L. P.; Bi, S.; Zhu, J. J. Cascade Amplification-Mediated In Situ Hot-Spot Assembly for MicroRNA Detection and Molecular Logic Gate Operations. *Anal. Chem.* **2018**, *90* (7), 4544-4551.

(13) Xiong, E.; Li, Z.; Zhang, X.; Zhou, J.; Yan, X.; Liu, Y.; Chen, J. A Triple-Helix Molecular Switch Electrochemical Ratiometric Biosensor for Ultrasensitive Detection of Nucleic Acids. *Anal. Chem.* **2017**, *89* (17), 8830-8835.

(14) Bao, T.; Wen, W.; Zhang, X.; Wang, S. An Exonuclease-Assisted Amplification Electrochemical Aptasensor of Thrombin Coupling "Signal on/off" Strategy. *Anal. Chim. Acta* **2015**, *860* (3), 70-76.

(15) Cao, X.; Xia, J.; Liu, H.; Zhang, F.; Wang, Z.; Lu, L. A New Dual-Signalling Electrochemical Aptasensor with the Integration of “Signal on/off” and “Labeling/Label-free” Strategies. *Sensor. Actuat. B-Chem.* **2017**, *239* (1), 166-171.

(16) Pei, H.; Liang, L.; Yao, G. B.; Li, J.; Huang, Q.; Fan, C. H. Reconfigurable Three-Dimensional DNA Nanostructures for the Construction of Intracellular Logic Sensors. *Angew. Chem. Int. Ed.* **2012**, *51* (36), 9020-9024.

(17) Xiong, E.; Wu, L.; Zhou, J.; Yu, P.; Zhang, X.; Chen, J. A Ratiometric Electrochemical Biosensor for Sensitive Detection of Hg^{2+} Based on Thymine-Hg^{2+}-Thymine Structure. *Anal. Chim. Acta* **2015**, *853* (1), 242-248.

(18) Li, Y.; Chang, Y.; Ma, J.; Wu, Z.; Yuan, R.; Chai, Y. Programming A Target-Initiated Bifunctional DNAzyme Nanodevice for Sensitive Ratiometric Electrochemical Biosensing. *Anal. Chem.* **2019**, *91* (9), 6127-6133.

(19) Li, L.; Wang, L.; Xu, Q.; Xu, L.; Liang, W.; Li, Y.; Ding, M.; Aldalbahi, A.; Ge, Z.; Wang, L.; Yan, J.; Lu, N.; Li, J.; Wen, Y.; Liu, G. Bacterial Analysis Using an Electrochemical DNA Biosensor with Poly-Adenine-Mediated DNA Self-Assembly. *ACS Appl. Mater. Interfaces* **2018**, *10* (8), 6895-6903.

(20) Yu, Y. Y.; Chen, Z. G.; Jian, W. S.; Sun, D. P.; Zhang, B. B.; Li, X. C.; Yao, M. C. Ultrasensitive Electrochemical Detection of Avian Influenza a (H7N9) Virus DNA Based on Isothermal Exponential Amplification Coupled with Hybridization Chain Reaction of DNAzyme Nanowires. *Biosens. Bioelectron.* **2015**, *64* (3), 566-571.

(21) Cai, S.; Chen, M.; Liu, M.; He, W.; Liu, Z.; Wu, D.; Xia, Y.; Yang, H.; Chen, J. A Signal Amplification Electrochemical Aptasensor for the Detection of Breast Cancer Cell Via Free-Running DNA Walker. *Biosens. Bioelectron.* **2016**, *85*, 184-189.

(22) Cheng, H.; Liu, J.; Ma, W.; Duan, S.; Huang, J.; He, X.; Wang, K. Low Background Cascade Signal Amplification Electrochemical Sensing Platform for Tumor-Related mRNA Quantification by Target-Activated Hybridization Chain Reaction and Electroactive Cargo Release. *Anal. Chem.* **2018**, *90* (21), 12544-12552.

(23) Wang, K.; He, M. Q.; Zhai, F. H.; Wang, J.; He, R. H.; Yu, Y. L. Autonomous DNA Nanomachine Based on Cascade Amplification of Strand Displacement and DNA Walker for Detection of Multiple DNAs. *Biosens. Bioelectron.* **2018**, *105*, 159-165.

(24) Zhang, Y.; Yan, Y.; Chen, W.; Cheng, W.; Li, S.; Ding, X.; Li, D.; Wang, H.; Ju, H.; Ding, S. A Simple Electrochemical Biosensor for Highly Sensitive and Specific Detection of MicroRNA Based on Mismatched Catalytic Hairpin Assembly. *Biosens. Bioelectron.* **2015**, *68*, 343-349.

(25) Chu, C. J.; Yeh, C. S.; Liao, C. K.; Tsai, L. C.; Huang, C. M.; Lin, H. Y.; Shyue, J. J.; Chen, Y. T.; Chen, C. D. Improving Nanowire Sensing Capability by Electrical Field Alignment of Surface Probing Molecules. *Nano Lett.* **2013**, *13* (6), 2564-2569.
(26) Liu, Y. T.; Irving, D.; Qiao, W. Q.; Ge, D. B.; Levicky, R. Kinetic Mechanisms in Morpholino-DNA Surface Hybridization. *J. Am. Chem. Soc.* **2011**, *133* (30), 11588-11596.
(27) Kjallman, T. H. M.; Peng, H.; Soeller, C.; Travas-Sejdic, J. Effect of Probe Density and Hybridization Temperature on the Response of an Electrochemical Hairpin-DNA Sensor. *Anal. Chem.* **2008**, *80* (24), 9460-9466.
(28) Lei, Q. L.; Ren, C. L.; Su, X. H.; Ma, Y. Q. Crowding-Induced Cooperativity in DNA Surface Hybridization. *Sci. Rep.* **2015**, *5*, 9217.
(29) Peterson, A. W.; Heaton, R. J.; Georgiadis, R. M. The Effect of Surface Probe Density on DNA Hybridization. *Nucleic Acids Res.* **2001**, *29* (24), 5163-5168.
(30) Curtis, S. D.; Ploense, K. L.; Kurnik, M.; Ortega, G.; Parolo, C.; Kippin, T. E.; Plaxco, K. W.; Arroyo-Curras, N. Open Source Software for the Real-Time Control, Processing, and Visualization of High-Volume Electrochemical Data. *Anal. Chem.* **2019**, *91* (19), 12321-12328.
(31) Dauphin-Ducharme, P.; Arroyo-Curras, N.; Plaxco, K. W. High-Precision Electrochemical Measurements of the Guanine-, Mismatch-, and Length-Dependence of Electron Transfer from Electrode-Bound DNA Are Consistent with a Contact-Mediated Mechanism. *J. Am. Chem. Soc.* **2019**, *141* (3), 1304-1311.
(32) Gu, Q.; Nanney, W.; Cao, H. H.; Wang, H.; Ye, T. Single Molecule Profiling of Molecular Recognition at a Model Electrochemical Biosensor. *J. Am. Chem. Soc.* **2018**, *140* (43), 14134-14143.
(33) Soleymani, L.; Fang, Z.; Sargent, E. H.; Kelley, S. O. Programming the Detection Limits of Biosensors through Controlled Nanostructuring. *Nature Nanotech.* **2009**, *4* (12), 844-848.
(34) Lin, M.; Wang, J.; Zhou, G.; Wang, J.; Wu, N.; Lu, J.; Gao, J.; Chen, X.; Shi, J.; Zuo, X.; Fan, C. Programmable Engineering of a Biosensing Interface with Tetrahedral DNA Nanostructures for Ultrasensitive DNA Detection. *Angew. Chem. Int. Ed.* **2015**, *54* (7), 2151-2155.
(35) Fan, C.; Plaxco, K. W.; Heeger, A. J. Electrochemical Interrogation of Conformational Changes as a Reagentless Method for the Sequence-Specific Detection of DNA. *Proc. Natl. Acad. Sci. U. S. A.* **2003**, *100* (16), 9134-9137.
(36) Farjami, E.; Campos, R.; Ferapontova, E. E. Effect of the DNA End of Tethering to Electrodes on Electron Transfer in Methylene Blue-Labeled DNA Duplexes. *Langmuir* **2012**, *28* (46), 16218-16226.
(37) Abi, A.; Ferapontova, E. E. Unmediated by DNA Electron Transfer in Redox-Labeled DNA Duplexes End-Tethered to Gold Electrodes. *J. Am. Chem. Soc.* **2012**, *134* (35), 14499-14507.
(38) Ricci, F.; Lai, R. Y.; Heeger, A. J.; Plaxco, K. W.; Sumner, J. J. Effect of Molecular Crowding on the Response of an Electrochemical DNA Sensor. *Langmuir* **2007**, *23* (12), 6827-6834.
(39) Zhang, J.; Song, S.; Wang, L.; Pan, D.; Fan, C. A gold nanoparticle-based chronocoulometric DNA sensor for amplified detection of DNA. *Nat. Protoc.* **2007***, 2(11),* 2888-2895.
(40) Su, S.; Sun, H. F.; Cao, W. F.; Chao, J.; Peng, H. Z.; Zuo, X. L.; Yuwen, L. H.; Fan, C. H.; Wang, L. H. Dual-Target Electrochemical Biosensing Based on DNA Structural Switching on Gold Nanoparticle-Decorated MoS_2 Nanosheets. *ACS Appl. Mater. Interface* **2016**, *8* (11), 6826-6833.
(41) Zhang, J.; Song, S. P.; Zhang, L. Y.; Wang, L. H.; Wu, H. P.; Pan, D.; Fan, C. H. Sequence-Specific Detection of Femtomolar DNA via a Chronocoulometric DNA Sensor (CDS): Effects of Nanoparticle-Mediated Amplification and Nanoscale Control of DNA Assembly at Electrodes. *J.*

Am. Chem. Soc. **2006**, *128* (26), 8575-8580.
(42) Farjami, E.; Clima, L.; Gothelf, K.; Ferapontova, E. E. "Off-On" Electrochemical Hairpin-DNA-Based Genosensor for Cancer Diagnostics. *Anal. Chem.* **2011**, *83* (5), 1594-1602.
(43) Pang, J.; Zhang, Z.; Jin, H. Effect of Structure Variation of the Aptamer-DNA Duplex Probe on the Performance of Displacement-Based Electrochemical Aptamer Sensors. *Biosens. Bioelectron.* **2016**, *77*, 174-181.
(44) Anne, A.; Demaille, C. Dynamics of Electron Transport by Elastic Bending of Short DNA Duplexes. Experimental Study and Quantitative Modeling of the Cyclic Voltammetric Behavior of 3'-Ferrocenyl DNA End-Grafted on Gold. *J. Am. Chem. Soc.* **2006**, *128* (2), 542-557.
(45) Laviron, E. General Expression of the Linear Potential Sweep Voltammogram in the Case of Diffusionless Electrochemical Systems. *J. Electroanal. Chem.* **1979**, *101*, 19–28.

TOC

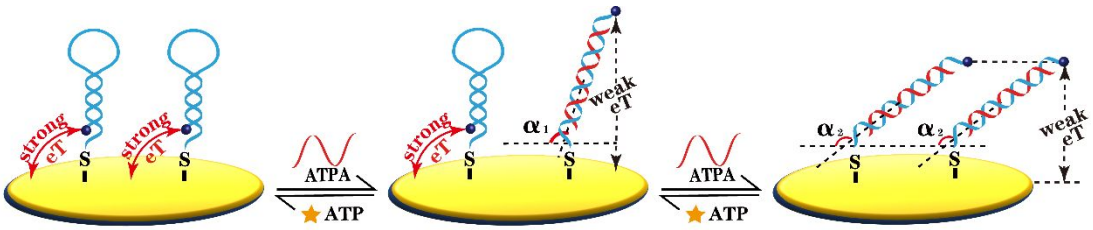
strong eT
S
strong eT
S
ATPA
ATP
strong eT
S
α1
S
weak eT
ATPA
ATP
α2
S
α2
S
weak eT